ANTIOXIDANTS & REDOX SIGNALING
Volume 14, Number 2, 2011

DOI: 10.1089/ars.2010.3266

ORIGINAL RESEARCH COMMUNICATION

The Effect of Small Changes in Hematocrit on Nitric Oxide Transport in Arterioles

Krishna Sriram,[1] Beatriz Y. Salazar Vázquez,[2] Ozlem Yalcin,[3] Paul C. Johnson,[3] Marcos Intaglietta,[3] and Daniel M. Tartakovsky[1]

Abstract

We report the development of a mathematical model that quantifies the effects of small changes in systemic hematocrit (Hct) on the transport of nitric oxide (NO) in the microcirculation. The model consists of coupled transport equations for NO and oxygen (O2) and accounts for both shear-induced NO production by the endothelium and the effect of changing systemic Hct on the rate of NO production and the rate of NO scavenging by red blood cells. To incorporate the dependence of the plasma layer width on changes in Hct, the model couples the hemodynamics of blood in arterioles with NO and O2 transport in the plasma layer. A sensitivity analysis was conducted to determine the effects of uncertain model parameters (the thicknesses of endothelial surface layers and diffusion coefficients of NO and O2 in muscle tissues and vascular walls) on the model's predictions. Our analysis reveals that small increases in Hct may raise NO availability in the vascular wall. This finding sheds new light on the experimental data that show that the blood circulation responds to systematic increases of Hct in a manner that is consistent with increasing NO production followed by a plateau. *Antioxid. Redox Signal.* 14, 175–185.

Introduction

Nitric oxide (NO) is a secretory product of mammalian cells that is thought to act as a key messenger in various physiological processes in central and peripheral nervous systems, the cardiovascular system, immune and inflammatory systems, and the like. (21). The physiologic importance of NO generated a large number of experimental and modeling studies (3) that vary in complexity and fidelity. In what is often considered to be the first mathematical model of NO endothelium production and hemoglobin scavenging, Lancaster (14) accounted for the intracellular and intercellular diffusion and reaction of free NO with oxygen (O2) and hemoglobin (Hb). This model was subsequently modified by Butler *et al.* (4) to account for the presence of a plasma layer (Fig. 1)—a region in the immediate vicinity of the endothelium in which blood contains no red blood cells (RBCs)—and to incorporate the scavenging effect of hemoglobin. A mathematical model (26) of interactions between hemoglobin O2 carriers and NO demonstrated the dependence of NO scavenging rates on hematocrit (Hct). Lamkin- Kennard *et al.* (13) further generalized these models by incorporating two mechanisms by which NO influences O2 transport to tissue: "O2 is required for NO production," and "tissue O2 consumption is reversibly inhibited by NO."

This study aims to elucidate the third mechanism in this complex phenomenon identified in refs. (3, 13): "interactions between NO and Hb influence blood flow and O2 delivery." Specifically, we investigate quantitatively how changes in Hct affect both NO production and scavenging and O2 transport. Physicochemical processes affecting this process are well understood. As Hct increases so does apparent blood viscosity (23) and shear stress at the vessel wall (26). This, in turn, leads to changes in the rate of NO production by the endothelium (1, 11, 19, 20, 24). Additionally, simulation results and experimental data show that the rate of NO scavenging increases with rising Htc (29).

While recognizing the importance of shear-stress-dependent NO production, two of the most recent and complete models of coupled NO/O2 transport (5, 9) do not account for this effect. Moreover, these models rely on assumed rather than rigorously derived velocity profiles. The parabolic velocity profile adopted in ref. (5) implies Poiseuille flow of a single-phase Newtonian fluid, which neglects the presence of a plasma layer. The plug-flow velocity profile used by both Chen *et al.* (5) and Gundersen *et al.* (9) assumes blood velocity

[1]Department of Mechanical and Aerospace Engineering, University of California, San Diego, La Jolla, California.
[2]Facultad de Medicina, Universidad Juárez del Estado de Durango, Durango, México.
[3]Department of Bioengineering, University of California, San Diego, La Jolla, California.

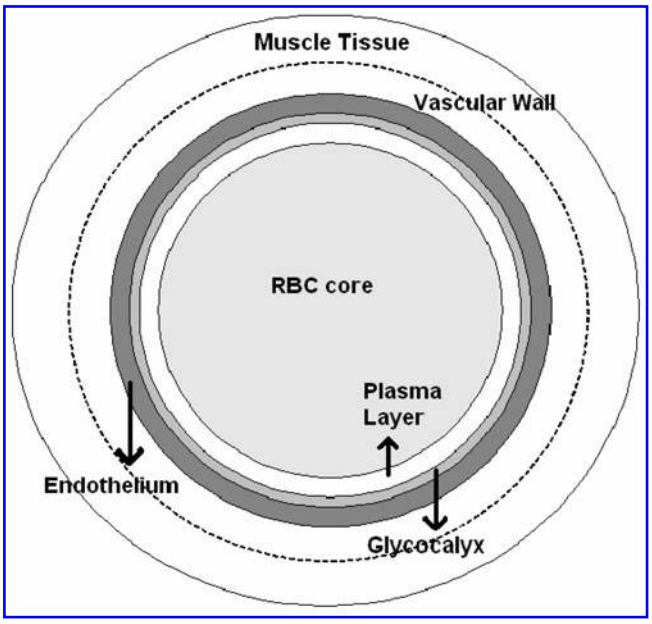

FIG. 1. Cross section of an arteriole. A version of the Krogh tissue cylinder model used in our analysis consists of RBC-rich core, RBC-free plasma layer, glycocalyx, endothelium, vascular wall, and smooth muscle tissue. RBC, red blood cell.

to be constant across the RBC-rich core and to vary linearly in the plasma layer. This leads to inaccurate predictions of shear stress at the wall, as can be seen from Figure 2.

The model of coupled NO/O2 transport we present below generalizes its current state-of-the-art counterparts (5, 9, 13) in the following ways. First, it employs a blood velocity profile that is rigorously derived from a representation of arteriolar hemodynamics as two-phase flow with the RBC-rich core and the RBC-free plasma layer (26). Second, it incorporates the experimentally observed dependence of NO endothelium production on shear stress. Third, it accounts for the theoretically derived [refs. (2, 27) and references therein] and experimentally observed (8, 15) differences between values of diffusion coefficients in free fluids (*e.g.*, plasma layer) and porous media (*e.g.*, glycocalyx and muscle tissue). Finally, experimental data (12, 33) are used to characterize the dependence of the plasma layer thickness on Hct, thus relating the blood hemodynamics to NO availability in smooth muscle tissue and vascular walls.

Our analysis is motivated in part by the experimental observations of Martini *et al.* (17, 18, 25), who found that small Hct increases in hamsters can lead simultaneously to lowered blood pressure and increased cardiac output. Gundersen *et al.* (9) postulated that this effect might be caused by vessel dilation due to increased shear-stress-induced NO production rather than due to increased O2 transport across the blood vessel wall. Our mathematical model supports this hypothesis.

Methods

Mathematical model

Model geometry. Following Lamkin-Kennard *et al.* (13), Chen *et al.* (5), and Gundersen *et al.* (9), among many others, we adopt a modified Krogh tissue cylinder model of an arteriole. This model idealizes an arteriole by a series of concentric cylinders representing (from the center outward): (a) RBC-rich core, (b) RBC-free plasma layer, (c) glycocalyx, (d) endothelium, (e) vascular wall, and (f) smooth muscle tissue (Fig. 1). Other versions of the Krogh tissue cylinder model can be used in the analysis below as well.

A cylindrical coordinate system (r, z) is used to describe coupled transport of NO and O2 in an arteriole. The two-phase blood flow is in the z direction, along the arteriole's length. To facilitate the comparison with the analyses in refs. (4, 9, 13, 14), that is, to elucidate the effects of shear-stress-dependent NO endothelium production on coupled NO and Hb transport and on resulting O2 delivery, we take the endothelium NO production to be uniform along the arteriole's length and set the concentrations of NO and O2 in the arteriole's inlet and outlet to be the same. This physiological setting is justified by both modeling results and experimental evidence. Specifically, numerical results of Chen *et al.* (5), whose model accounts for advective transport in an arteriole, demonstrates that the axial variability of these concentrations is negligibly small as long as NO production is uniform along the length of an arteriole. Experimental investigations of Intaglietta *et al.* (10) found the longitudinal (axial) O2 gradient measured in blood micro-vessels to be very small (on the order of 8 mmHg/cm).

Under these conditions, both NO concentration C_{NO} and O2 partial pressure P_{O2} vary in the radial (r) direction only, so that $\mathbf{u} \cdot \nabla C_{NO} \equiv 0$ and $\mathbf{u} \cdot \nabla P_{O2} \equiv 0$, where $\mathbf{u}$ is the blood velocity vector whose only nonzero component u is in the z direction. This leaves diffusion and reactions in the radial

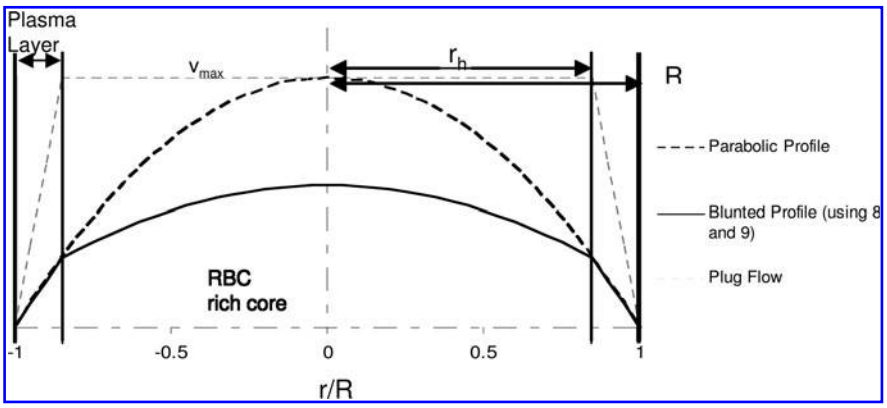

FIG. 2. Blood velocity profiles corresponding to the two-phase flow model and their parabolic and plug-flow counterparts used in the previous analyses (5, 9).

direction as the only transport mechanisms. These are described by a system of coupled steady-state reaction–diffusion equations (5, 9, 13) presented below.

Transport equations.

RBC-rich core ($0 < r < r_h$). In this region, O2 partial pressure P_{O2} is constant and NO concentration C_{NO} satisfies a steady-state reaction–diffusion equation,

$$\frac{D_{NO}}{r}\frac{\partial}{\partial r}\left(r\frac{\partial C_{NO}}{\partial r}\right) - \lambda_b C_{NO} = 0. \quad [1]$$

Here D_{NO} is the diffusion coefficient of NO in the RBC-rich core, and λ_b is the reaction rate constant of NO scavenging by RBCs. The latter varies linearly with Hct (5, 9, 29), $\lambda_b = \lambda_0$Hct, where λ_0 is the value of λ_b at the reference value of Hct (45%).

Plasma layer ($r_h < r < R$) and glycocalyx ($R < r < r_g$). Owing to the absence of RBCs in plasma layer, no biochemical reactions occur in either plasma layer or glycocalyx. Hence, NO concentration C_{NO} and O2 partial pressure P_{O2} satisfy steady-state diffusion equations

$$\frac{D_{NO}}{r}\frac{\partial}{\partial r}\left(r\frac{\partial C_{NO}}{\partial r}\right) = 0 \quad [2]$$

and

$$\frac{\alpha D_{O2}}{r}\frac{\partial}{\partial r}\left(r\frac{\partial P_{O2}}{\partial r}\right) = 0, \quad [3]$$

respectively. Here α denotes the O2 solubility, and the diffusion coefficients of NO (D_{NO}) and O2 (D_{O2}) in plasma layer are larger than their counterparts in glycocalyx (8, 15).

Endothelium ($r_g < r < r_e$). Assuming that the rate of O2 consumption is twice the rate of NO production (5), C_{NO} and P_{O2} satisfy a coupled system of steady-state reaction–diffusion equations

$$\frac{D_{NO}}{r}\frac{\partial}{\partial r}\left(r\frac{\partial C_{NO}}{\partial r}\right) + R_e = 0 \quad [4]$$

and

$$\frac{\alpha D_{O2}}{r}\frac{\partial}{\partial r}\left(r\frac{\partial P_{O2}}{\partial r}\right) - 2R_e = 0. \quad [5]$$

The reaction rate R_e is assumed to follow Michaelis–Menten kinetics (3),

$$R_e = \frac{R_{NO,\max} P_{O2}}{P_{O2} + K_M}, \quad [6]$$

where K_M is the Michaelis–Menten constant. We allow the maximum reaction rate $R_{NO,\max}$ to vary with shear stress at the vessel wall, as discussed later. This dependence enables our model to account for the effect of shear stress on NO production.

Vascular wall ($r_e < r < r_w$) and smooth muscle tissue ($r_w < r < r_m$). Following (3), we assume that NO undergoes a pseudo first-order reaction with reaction rate constant λ_t, and that O2 consumption is inhibited by NO and follows Michaelis–Menten kinetics. The corresponding transport equations take the form

$$\frac{D_{NO}}{r}\frac{\partial}{\partial r}\left(r\frac{\partial C_{NO}}{\partial r}\right) - \lambda_t C_{NO} = 0 \quad [7]$$

$$\frac{\alpha D_{O2}}{r}\frac{\partial}{\partial r}\left(r\frac{\partial P_{O2}}{\partial r}\right) - R_m = 0, \quad [8]$$

where peak O2 consumption rate $R_{O2,\max}$ is lower in the vascular wall than in the muscle tissue, and (3)

$$R_m = \frac{R_{O2,\max} P_{O2}}{P_{O2} + K_M^m}, \quad K_M^m = 1 + \frac{C_{NO}}{27\text{nM}}.$$

Boundary conditions. Transport equations [1]–[8] are subject to the following boundary conditions. NO concentration C_{NO} is symmetric about the arteriole center $r = 0$,

$$\frac{\partial C_{NO}}{\partial r}(r = 0) = 0. \quad [9]$$

We assume that both C_{NO} and P_{O2} reach their respective asymptotic in the vicinity of the outer boundary of the muscle tissue $r = r_m$, so that (13)

$$\frac{\partial C_{NO}}{\partial r}(r = r_m) = 0, \quad \frac{\partial P_{O2}}{\partial r}(r = r_m) = 0. \quad [10]$$

Mass conservation across the interfaces between adjacent layers requires that

$$C_{NO}^- = C_{NO}^+,\ P_{O2}^- = P_{O2}^+,\ \left(D_{NO}\frac{\partial C_{NO}}{\partial r}\right)^- = \left(D_{NO}\frac{\partial C_{NO}}{\partial r}\right)^+,\ \left(D_{O2}\frac{\partial P_{O2}}{\partial r}\right)^- = \left(D_{O2}\frac{\partial P_{O2}}{\partial r}\right)^+, \quad [11]$$

where the superscripts minus and plus indicate that the corresponding quantities are computed, respectively, inside and outside of each interface shown in Figure 1.

It is worthwhile emphasizing that, if and when physiologically appropriate, this model can readily be generalized to account for axial variability of the concentrations of NO and O2 by adding the advective terms $\mathbf{u}\cdot\nabla C_{NO} \equiv 0$ and $\mathbf{u}\cdot\nabla P_{O2} \equiv 0$ to equations [1]–[2] and [3], respectively. Such a generalization of the transport model 1–11 is important for tackling spatially variable NO production, for example, NO production from neuronal NOS, but lies outside the scope of the present analysis and is left for follow-up studies.

Blood flow velocity and shear stress. All previously described models of coupled NO and O2 transport implicitly employ a two-phase model of blood flow in a cylinder of constant diameter (26). The first fluid (phase) is the RBC-rich core and has viscosity μ_c; the second phase is plasma that has viscosity μ_p. These two phases are assumed to be immiscible.

Assuming steady-state fully developed flow in the inertial regime, Stokes equations yield velocities of the core, u_c, and plasma, u_p (26),

$$u_c(\xi) = \frac{JR^2}{4\mu_p}\left[1 - \lambda^2 + \frac{\mu_p}{\mu_c}(\lambda^2 - \xi^2)\right]_{\text{for } 0 \le \xi \le \lambda} \quad [12]$$

$$u_p(\xi) = \frac{JR^2}{4\mu_p}(1 - \xi^2)_{\text{for } \lambda \le \xi \le 1}. \quad [13]$$

Velocity profiles [12] and [13] are written in the dimensionless coordinate system $\xi = r/R$ with $\lambda = r_h / R$; and $J = (P_i - P_o)/L$ is the pressure gradient along the arteriole of length L with entry and exit pressures P_i and P_o, respectively. Figure 2 presents the velocity profiles [12] and [13] and compares them with the parabolic and plug-flow velocity profiles used in the previous analyses (5) and (9). The parameter values used are presented in Table 1.

Flow rate Q is obtained by integrating the velocity profile given by expressions 12 and 13 over the cross section of the arteriole with dimensionless radius $\xi = 1$,

$$Q = \frac{\pi JR^4}{8\mu_p}\left(\frac{\mu_p}{\mu_c}\lambda^4 + 1 - \lambda^4\right). \quad [14]$$

Table 1. Values of Parameters Used in Simulations

Parameter	*Symbol used*	*Value*	*Reference*
Solubility of O2	α	1.34 Mm/torr	13
Diffusivity of O2 in fluid layers	D_{O2}	2800 $\mu m^2/s$	13
Diffusivity of NO in fluid layers	D_{NO}	3300 $\mu m^2/s$	14
Diffusivity of O2 in solid layers	D_{O2}	2800 or 1400 $\mu m^2/s$	8, 15
Diffusivity of NO in solid layers	D_{NO}	3300 or 1650 $\mu m^2/s$	
Maximum O2 consumption rate in tissue	$R_{O2,max}$	20 $\mu M/s$	5
Maximum NO production rate in endothelium	$R_{NO,max}$	150 $\mu M/s$	5
Scavenging rate of NO in blood at 45% hematocrit	λ_b	382.5 s^{-1}	2, 27
Rate of consumption of NO in tissue	λ_t	1 s^{-1}	13
Michaelis–Menten constant for NO in endothelium	K_M	4.7	3
Ratio of diffusivities in solid and liquid phases	D_r	1, 1/2	
Arteriole diameter (*i.e.*, fluid domain)	R	20 μm	13
Glycocalyx		0.25–1 μm	31
Endothelium		1 μm	
Smooth muscle tissue		80 μm	5

O2, oxygen; NO, nitric oxide.

It follows from expression [13] that shear stress τ at the wall, $\xi = 1$, is given by

$$\tau = \frac{JR}{2}. \quad [15]$$

Combining expressions [13] and [14] yields

$$\tau = \frac{4\mu_p Q}{\pi R^3}\left(\frac{\mu_p}{\mu_c}\lambda^4 + 1 - \lambda^4\right)^{-1}. \quad [16]$$

Equation [16] expresses shear stress τ in terms of blood viscosity μ_p and the width of plasma layer $\delta = (1 - \lambda)R$.

Shear-stress-dependent NO production. In our model, changes in Hct affect the shear stress τ in equation [16] *via* the dependence on Hct of both blood viscosity, $\mu_c = \mu_c$ (Hct), and the width of plasma layer, $\delta = \delta$(Hct). The model is capable of accommodating any phenomenological relations (constitutive laws). To be concrete, we employ:

1. a linear relationship $\mu_c = \mu_c$(Hct) suggested by the experimental data reported in ref. (17); and
2. a linear relationship between δ and systemic Hct H_d suggested by the experimental data presented in the Appendix.

Specifically, the Martini *et al.* (17) viscometry data suggest that in the physiological range of Hct

$$\mu_c = a_1 \text{Hct} + a_2 \quad [17]$$

where $a_1 = 0.1678$ and $a_2 = -4.348$ cp. The experimental data presented in the Appendix lead to

$$\delta = a_3 H_d + a_4 \quad [18]$$

with $a_3 = -7.55\mu m$ and $a_4 = 6.91\mu m$. The core (Hct) and systemic (H_d) Hcts are related through mass conservation of RBCs (13),

$$\text{Hct}\int_0^{\lambda} u_c(\xi)\xi d\xi = H_d\left[\int_0^{\lambda} u_c(\xi)\xi d\xi + \int_{\lambda}^{1} u_p(\xi)\xi d\xi\right]. \quad [19]$$

For the velocity profile given by expressions [12] and [13], this gives

$$H_d = 2\text{Hct}\lambda^2\left(1 - \lambda^2 + \lambda^2\frac{\mu_p}{2\mu_c}\right)\left(1 - \lambda^2 + \lambda^2\frac{\mu_p}{\mu_c}\right)^{-1}. \quad [20]$$

Equation [20] is nonlinear, since $\lambda(H_d) = 1 - \delta(H_d)/R$ where $\delta(H_d)$ given by the linear relation [18]. This equation can be approximated by a linear relation

$$\text{Hct} = a_5 H_d + a_6 \quad [21]$$

with $a_5 = 0.9608$ and $a_6 = 0.1012$ for the arteriole radius $R = 20\,\mu m$. This linear fit is very accurate within the physiological range of Hct being studied (from around 35 to 55) with $R^2 = 0.998$.

Recalling that $\lambda = 1 - \delta/R$, and substituting relations [17], [18], and [21] into expression [16], we obtain a closed-form relation between shear stress τ and systemic Hct H_d,

$$\tau = \frac{4\mu_p Q}{\pi R^3}\left[\frac{\mu_p \lambda^4}{a_1(a_5 H_d + a_6) + a_2} + 1 - \lambda^4\right]^{-1}, \quad \lambda = 1 - \frac{a_3 H_d + a_4}{R}. \qquad [22]$$

The variation of shear stress with systemic Hct given by equation [22] is plotted in Figure 3, in the range of Hct considered in this study (and for a vessel diameter of 40 μm); the relationship is well described with a straight line (Fig. 3). We consider a range of systemic Hct values from 35% to 55%, and normalize the shear stress with the shear stress calculated at 55% Hct.

Experimental data (1, 11, 19, 20, 24) suggest that the rate of NO production by the endothelium increases with shear stress. We model this effect by allowing the maximum NO production rate $R_{NO,\max}$ in the Michaelis–Menten kinetics law [6] to vary with shear stress τ according to

$$R_{NO,\max}(\tau) = f(\tau) R^*_{NO,\max}, \qquad [23]$$

where $f(\tau) \leq 1$ is a positive monotonically increasing function, and $R^*_{NO,\,\max}$ is the maximum NO production rate reached at $\tau = \tau^*$, such that $f(\tau^*) = 1$ and $R_{NO,\max}$ remains constant ($R^*_{NO,\,\max}$) for $\tau \geq \tau^*$.

To be specific, we employ a logistic (S-shaped) curve suggested by experimental data in ref. (6),

$$f(\tau) = \tanh\,(\pi \tau^m), \qquad [24]$$

where the exponent m is a real number that determines how fast the curve approaches its asymptote $f(\tau^*) = 1$. Another possibility, which we do not pursue here because it has a kink at $\tau = \tau^*$, is to choose $f(\tau)$ to be linear (20). Figure 4 exhibits the maximum NO production rate predicted with relations [23] and [24] (Fig. 4a) and observed experimentally in ref. (6) (Fig. 4b). Shear stress is normalized with respect to its counterpart at the 55% systemic Hct.

The exponent m in relation [24] determines the width of the transitional zone between the minimum and maximum NO production by the endothelium. The experimental data (6) on the dependence of the activation of endothelial NO synthase on shear stress suggest that the width of this zone, and hence the value of m, can be highly variable and requires further experimental attention. Unless otherwise noted, the simulations reported below correspond to $m = 5$. We also explore the effect of choosing other values of m.

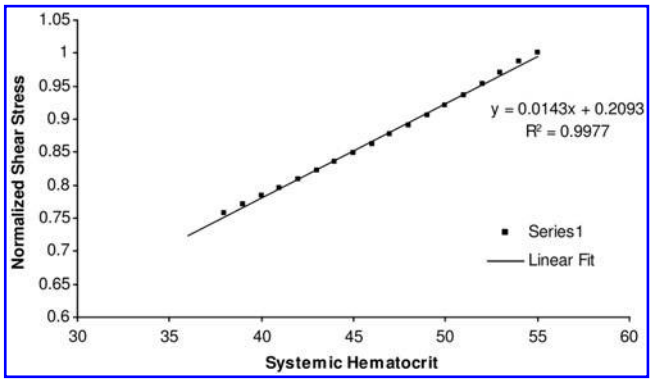

FIG. 3. Relationship between shear stress and systemic Hct for a vessel diameter of 40 νm (calculated using equation [22]). Hct, hematocrit.

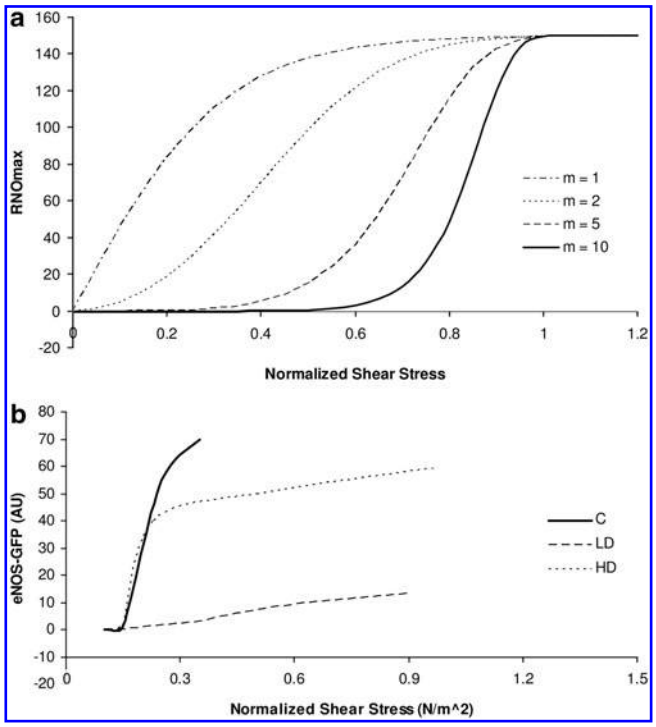

FIG. 4. Dependence of (a) $R_{NO,\max}$ on shear stress for different values of the exponent m, and (b) eNOS activation on shear stress, for different dosages of rampmycin in mice. C, control; LD, low dosage; HD, high dosage. Experimental data from ref. (6). AU signifies arbitrary units used by the authors of ref. (6) to quantify eNOS activation. NO, nitric oxide.

The proposed model of shear-stress-dependent NO production and coupled NO/O2 transport can be represented with the following algorithm. First, expression [19] is used to compute shear stress on the arteriole wall for a given level of Hct. Second, relations [23] and [24] are used to obtain the corresponding maximum NO production rate. Third, equations [1]–[11] are solved numerically to simulate the coupled NO/O2 transport in the arteriole.

Model parameterization. The vast majority of the existing analyses of coupled NO/O2 transport employ the same values of diffusion coefficients D_{NO} and D_{O2} in all layers of the Krogh tissue cylinder model of arterioles. In a typical example (14), diffusion data for an aqueous solution (16) are used to select the values $D_{NO} = 3300\ \mu m^2/s$ and $D_{O2} = 2800\ \mu m^2/s$ for both fluid (RBC-rich core and plasma layer) and solid (glycocalyx, endothelium, vascular wall, and smooth muscle tissue) layers of the computational domain. Chen *et al.* (5) assumed D_{NO} and D_{O2} in the glycocalyx to be 10 times smaller than their counterparts in all other layers. The data reported in

refs. (8, 15) put the diffusion coefficient of O2 in muscle tissue at $D_{O2} = 1400\,\mu m^2/s$, that is, half the value of its counterpart in a free solution. Therefore, we take D_{NO} and D_{O2} in the solid layers to be half of those in the fluid layers. We also compare this with the assumption used in the previous studies, according to which D_{NO} and D_{O2} are constant throughout the computational domain. The values of these and other parameters used in our simulations are presented in Table 1.

Summary of modeling assumptions

- Blood flow is treated as a two-phase flow, with the phases being immiscible and Newtonian.
- Flow rate in the arteriole is constant.
- Linear relationship for blood viscosity *versus* Hct.
- The rate of scavenging of NO by RBCs increases linearly with Hct.
- Each individual layer is homogeneous.
- The simulation is carried out in steady state.
- Linear relationship between plasma layer thickness and systemic Hct.
- The blood vessel has constant diameter.
- Linear relationship between NO scavenging rate and Hct.

Numerical solution

We used a finite difference method to solve the system of coupled reaction–diffusion equations [1]–[11]. A method of discontinuous coefficients (30) is used at all interfaces between the adjacent layers (Fig. 1) to obtain suitable finite difference formulae. The equations were discretized using a second-order central difference scheme, and the resulting finite difference matrix equations were solved with the Thomas algorithm (22).

The system of coupled ordinary differential equations was solved iteratively as follows. First, the simulation is initialized with zero NO concentration everywhere, and O2 partial pressure constant across the RBC core and zero everywhere else. Second, the transport equations for O2 are solved, to obtain an initial O2 partial pressure profile. Third, the transport equations for NO are solved. Fourth, the O2 profile is recalculated, and the procedure is repeated until convergence criteria are met. As a convergence criterion, we chose the relative error in calculated NO profiles (*i.e.*, the maximum relative error of calculated NO concentration between successive iterations) to be less than 10^{-6}. Due to the relatively weak coupling between the systems of transport equations for NO and O2, the convergence was obtained after a relatively small number of iterations. The numerical code is written in MATLAB.

Simulation Results

The simulation results presented below aim to elucidate the importance of (a) variable Hct, (b) spatially varying diffusion coefficients of NO and O2 in the tissue and the blood stream, and (c) shear-induced NO production. These three effects are explored below in the order of the complexity of the underlying model.

We begin by isolating the effects that different levels of Hct have on NO production. This is done by keeping $R_{NO,max}$ constant (*i.e.*, by assuming that NO production is independent of shear stress) and assuming that diffusion coefficients in all layers shown in Figure 1 are the same. These assumptions correspond to the current state of the art in NO transport modeling (5, 9, 13). Figure 5 shows the resulting distributions of NO concentration C_{NO} and O2 partial pressure P_{O2} for three levels of systemic Hct. Increasing Hct causes an appreciable rise in P_{O2} (Fig. 5b), while its effects on C_{NO} are much less pronounced (Fig. 5a). Regardless of the Hct level, C_{NO} near the centerline of the vessel, $r \cong 0$, is close to 0 because NO is scavenged by RBCs; the level of NO drops steadily across the smooth muscle where NO is consumed according to the kinetics described by equation [7]. The levels of O2 gradually decrease, as it is consumed by the endothelium, vascular wall, and the smooth muscle tissue. O2 consumption in the tissue is impeded by high NO concentrations, in accordance with equation [7]. This general behavior of both C_{NO} and P_{O2} is in accordance with previous findings, for example, refs. (5, 9, 13).

Next, we incorporate the effects of variability of the diffusion coefficients D_{NO} and D_{O2} between the fluid (the RBC core and plasma layer) and solid (the endothelial surface layer, endothelium, and tissue) layers of the modified Krogh tissue cylinder model of an arteriole (Fig. 1). To be concrete, we set the ratio between the solid and fluid diffusion coefficients to $D_r = 0.5$. The resulting distributions of C_{NO} and P_{O2} are shown in Figure 6. The qualitative behavior of the two concentrations remains unchanged, but their profiles become steeper. Comparison of Figures 5 and 6 reveals that accounting for reduced diffusion coefficients in the tissue leads to higher peak NO concentrations in the vascular wall and to sharper decreases of availability of both NO and O2 with the distance from the

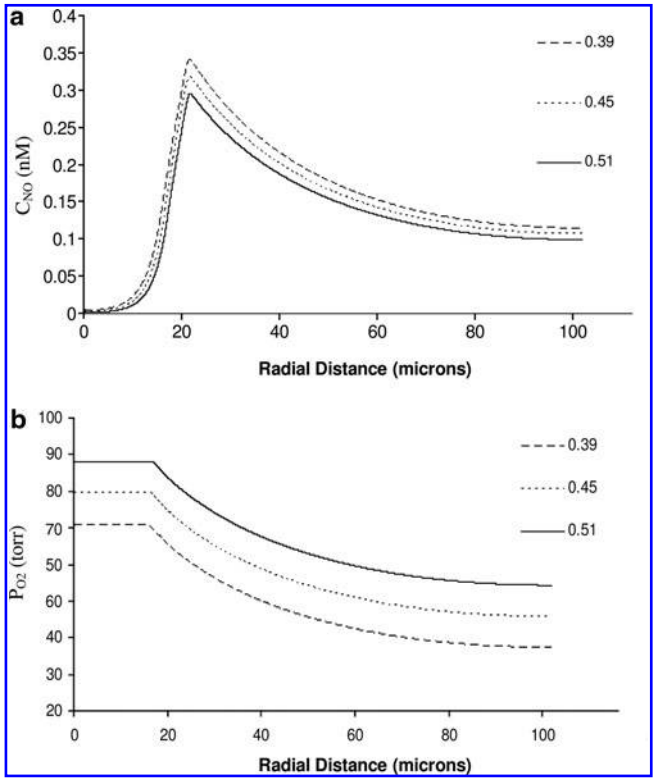

FIG. 5. Profiles of (a) NO concentration and (b) O2 partial pressure for several systemic Hct with the diffusion coefficients of NO and O2 same in all layers. O2, oxygen.

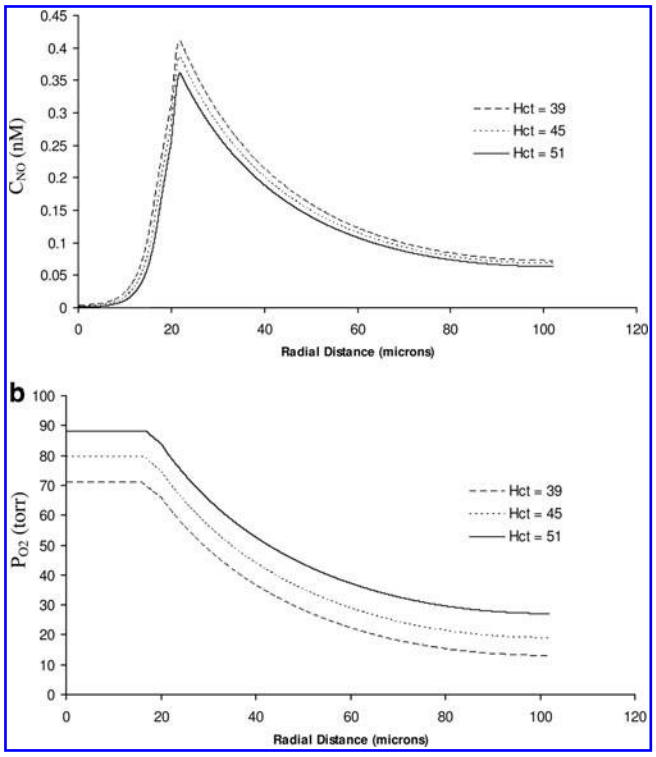

FIG. 6. Profiles of (a) NO concentration and (b) O2 partial pressure for several systemic Hct. The model with fixed $R_{NO,\max}$ and the variable diffusion coefficients ($D_r = 0.5$).

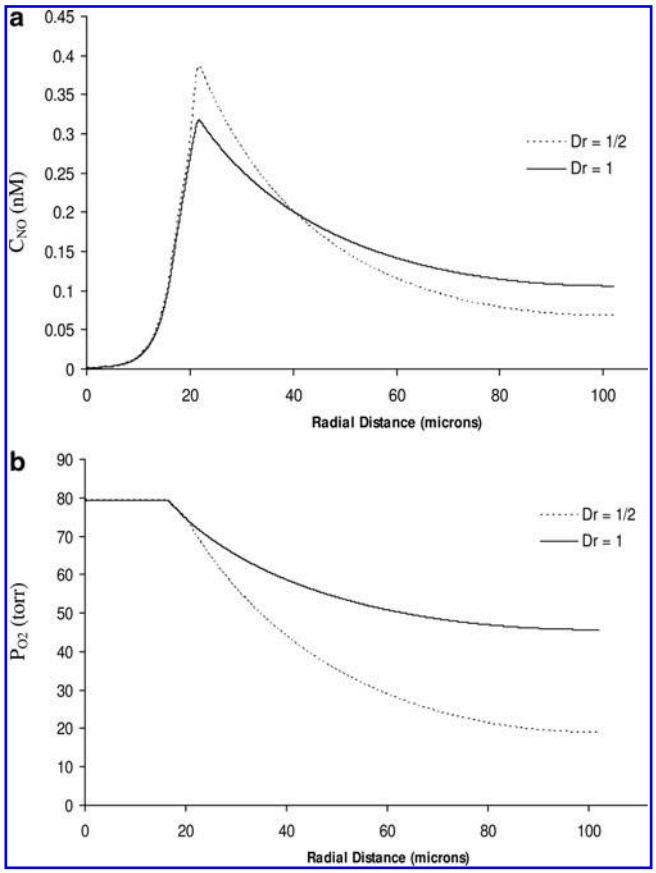

FIG. 7. Profiles of (a) NO concentration and (b) O2 partial pressure for 45% systemic Hct, with the model that accounts for the spatial variability of the diffusion coefficients ($D_r = 0.5$, *dotted lines*) and with model that ignores their variability (*solid lines*).

blood vessel. Figure 7 facilitates this comparison by plotting the C_{NO} and P_{O2} profiles at 45% Hct, computed with the model that accounts for the spatial variability of the diffusion coefficients (the dotted lines) and with the model that ignores their variability (solid lines).

According to Figures 5a and 6a, the coupled NO/O2 model with the fixed value of $R_{NO,\max}$ predicts that the peak NO concentration in the vascular wall declines as systemic Hct increases. While not shown here, we found this decrease to be monotonic and nearly linear. This behavior is due to the nonlinear interplay of the following three phenomena. First, increasing Hct causes the rate of NO consumption by the RBC core to rise. Second, increasing Hct reduces the plasma layer thickness, thereby reducing the distance NO must diffuse before being consumed by the RBCs in the core. Third, increasing Hct raises O2 availability, thus increasing NO production rates in accordance with equation [7]. The first two mechanisms contribute to the reduction of NO availability, and their combined effect on NO availability is only slightly offset by the third factor.

Finally, we consider the general version of our model, which also incorporates a shear dependence of NO production. Figure 8 exhibits the spatial distributions of C_{NO} and P_{O2} computed with this model for several values of systemic Hct and the diffusion coefficients ratio $D_r = 0.5$. Figure 8a suggests that the shear-dependent NO production exhibits a qualitatively different relationship between peak NO concentration and systemic Hct: NO availability in the vascular wall appears to *increase* with Hct.

Figures 9 and 10 explore this behavior in detail. Figure 9 shows the relationship between peak C_{NO} and systemic Hct for several values of the exponent m in the constitutive equation [24]. For $m = 5$ used in the simulations presented in Figure 8 (and other values of m as small as 2), the C_{NO}-Hct relationship exhibits an inflection point, at which C_{NO} reaches its maximum and then starts to decrease. This is due to the asymptotic behavior of $R_{NO,\max}$ (see the constitutive equation [24] and/or Figure 3a). In this limit, further increases in shear stress (and Hct) do not affect NO production and the increased consumption of NO by RBCs is no longer compensated by increasing shear-induced NO production, thus causing NO availability to decrease beyond the inflection point. The exponent m in the constitutive equation [24] determines its steepness and, hence, the rate at which NO production varies with shear stress. Larger values of the parameter m correspond to a steeper increase in NO production with shear stress and, hence, to a sharper increase in NO availability with rising Hct. Figure 10 confirms that this behavior remains essentially the same for different values of the glycocalyx thickness (in these simulations we set $m = 5$).

The following mechanisms combine to produce the nonlinear relationship between C_{NO} and Hct.

1. The rate of NO consumption by the RBC core increases with Hct.

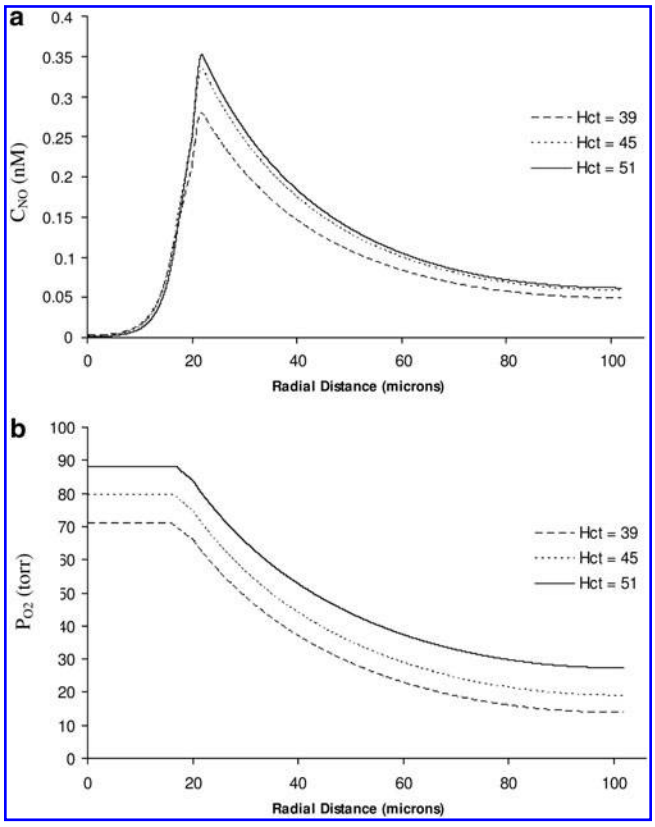

FIG. 8. Profiles of (a) NO concentration and (b) O2 partial pressure for several systemic Hct. The model with shear-dependent $R_{NO,max}$ (equation [24] with $m = 5$) and the variable diffusion coefficients ($D_r = 0.5$).

2. Blood viscosity and shear stress at the vessel wall increase with Hct.
3. O2 availability and NO production rates increase with Hct (equation [7]).
4. The thickness of the plasma layer decreases and shear stress increases with Hct (equation [16]).
5. The distance NO must diffuse before being consumed by RBCs in the core decreases with Hct.

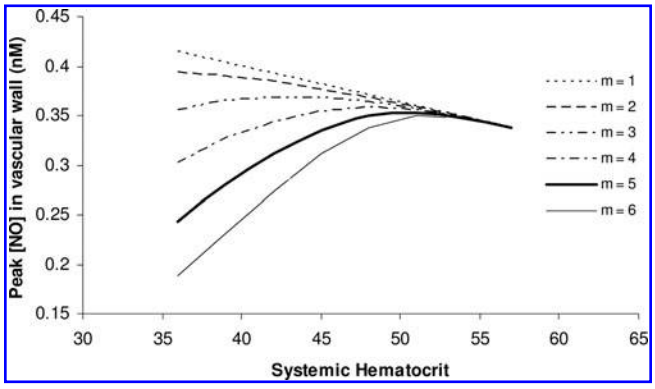

FIG. 9. The dependence of peak NO concentration on systemic Hct predicted by the shear-dependent NO production model with the constitutive equation [24] and several values of the exponent *m*.

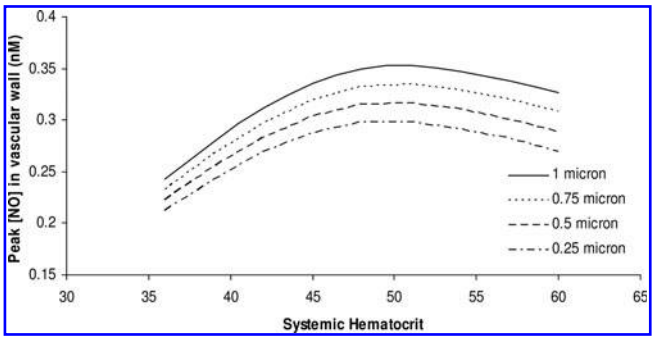

FIG. 10. The dependence of peak NO concentration on systemic Hct for several values of glycocalyx thickness.

Effects 2, 3, and 4 cause NO availability to increase, whereas effects 1 and 5 have the opposite effect. Interaction of these competing effects results in the behavior shown in Figures 9 and 10. It is worthwhile emphasizing that changes in the relative strengths of any of these phenomena may have quantitative and qualitative effects on the final relationship between NO availability in the vascular wall and systemic Hct.

Summary and Discussion

The principal result of our analysis is to elucidate and quantify mechanisms by which changes in Hct affect the NO availability in the vascular wall of arterioles. Using the two-phase blood flow model (26), we have shown how the relationship between NO production and shear stress affects the overall behavior of the system for different levels of Hct.

Theoretical reasoning and experimental evidence suggest that diffusion coefficients for solutes undergoing diffusion in porous media must be smaller than their counterparts in free

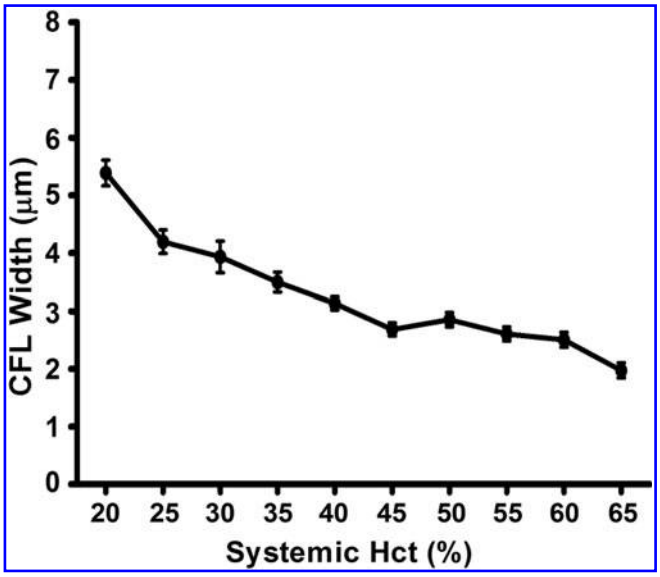

FIG. 11. Plasma layer (cell-free layer or CFL) width as a function of systemic Hct in rat cremaster muscles arterioles of 20–30 *v*m diameter.

fluids. We explored the effects different diffusion coefficients for NO and O2 in the fluid (the RBC core and plasma layer) and solid (the endothelial surface layer, endothelium, and tissue) layers of the modified Krogh tissue cylinder model of an arteriole have on coupled NO/O2 transport. Reduced diffusion coefficients in the tissue cause NO concentration (C_{NO}) in the vascular wall to increase. This suggests that NO produced by the endothelium may be even more important than previously thought in controlling vascular tone.

Examination of the O2 partial pressure (P_{O2}) distributions reveals that the resulting profiles for the cases, where shear-induced NO production is (a) ignored, and (b) taken into account are very similar, due to the weak coupling of NO and O2 transport. The strength of this coupling is determined by the parameters describing the Michaelis–Menten kinetics of NO production in the endothelium and O2 consumption in the vascular wall and tissue. Hence, the transport of O2 in the microcirculation can be evaluated without considering influences such as shear-induced NO production to a good first approximation.

The relationship between NO production and shear stress has been documented in previous studies (5, 6, 19, 20). However, there is as yet no definitive conclusion on the functional relationship between these quantities, especially *in vivo*, at physiological levels of shear stress. We used a constitutive relation (a logistic or S-shaped curve) to describe a relation between the maximum NO production by the endothelium and fluid shear stress at the vessel wall. Figure 9 demonstrates that this relationship has a significant effect on the resulting behavior of the system for different levels of systemic Hct. This suggests the need for additional investigations, both theoretical and experimental, either to better parameterize this constitutive law or to replace it with a physicochemical model based on the first principles, or both.

We demonstrated that relatively small changes in systemic Hct may significantly raise C_{NO} in the vascular wall. This has implications for NO production by the endothelium on vascular tone. Martini *et al.* (17, 18) found that the increase in Hct can result in decreased blood pressure. Our study suggests that changing Hct can potentially cause C_{NO} in the vascular wall to increase, thereby causing vasodilation. This may result in a net reduction in blood pressure even as Hct rises, as the resulting vasodilation compensates for increases in blood viscosity as Hct increases.

It has been suggested that the glycocalyx is crucial in mechanotransduction of shear stress from the blood flow in the lumen to the endothelium (32). Therefore, the current approach of relating NO production to shear stress at the wall may be an oversimplification of a more complex biomechanical system. This is particularly important considering the variety of glycocalyx thicknesses reported in the literature. Our study indicates that greater glycocalyx thicknesses result in higher C_{NO} in the vascular wall, a result consistent with Chen *et al.* (5). The resulting higher C_{NO} is because the glycocalyx acts as a barrier for NO diffusion from the endothelium to the blood stream, thereby reducing scavenging rates. This is offset slightly by the impedance of O2 diffusion from bloodstream to the tissue, which slightly alters NO production rates by the endothelium.

The rheological model (26) used in our study is a simplification of hemodynamics in small blood vessels. Blood flow in vessels of small diameter is generally non-Newtonian and shear-rate-dependent (7). Hence, while our present model highlights the methodology for correlating blood rheology with shear stress, future work will focus on the development of more realistic rheological models and their application to the shear-dependent coupled NO/O2 transport model presented in this paper.

Following the standard practice in the field (5, 9, 13), we did not model vasodilation, assuming that the vessel wall does not respond to changes in $C_{NO.}$This is a major simplification since smooth muscle in the arteriolar wall responds to changes in both C_{NO} and P_{O2} due to varied O2 carrying capacity induced by changes in Hct. An additional simplification is that blood flow is constant, and is not affected by the change of blood viscosity caused by varying Hct. Experimental data from awake hamsters subjected to small changes in Hct illustrates the complex behavior of the vascular compartment when Hct varies (25). These results, obtained with Hct variations implemented with O2 carrying and noncarrying RBCs, show that the circulation appears to behave according to conditions where increasing Hct produces a maximum NO concentration at a specific Hct. At this C_{NO} peripheral vascular resistance and peripheral vascular hindrance (vascular resistance independent of the effects of blood viscosity) reach their minima, which should be indicative of maximal dilatation. Finally, our model only deals with the endothelium as an NO source; however, the circulation presents additional potential sources of NO (28) such as those derived from cellular or acellular hemoglobin, which must eventually be accounted for in this type of analysis.

In conclusion, this model shows that comparatively small variations of Hct can affect NO concentration in the vascular wall of arterioles due to changes in the competition between NO production by shear stress and NO consumption by Hb in RBCs. The resulting balance of NO concentration in the vascular wall is strongly dependant on the relationship between NO production by the endothelium and shear stress. Exploration of the functional dependence of NO on shear stress and comparison with results from studies where Hct was systematically varied within a comparatively small range supports the suggestion that the circulation as a whole appears to behave as if NO bioavailability increases as Hct is increased before reaching a point of inflection.

Characterization of Plasma Layer Thickness as a Function of Variations in Hct

The plasma layer thickness was measured in the rat cremaster muscle preparation (33) according to the technique of Kim *et al.* (12). Hct was varied using either plasma or packed RBCs, from blood donors, for isovolemic hemodilution or hemoconcentration, respectively. Figure 11 shows the data used in our simulation.

Acknowledgments

This study was supported in part by the USPHS Bioengineering Research Partnership grant R24-HL 064395 (M.I.), R01-HL 062354 (M.I.), and R01-HL 076182 (P.C.J.).

Author Disclosure Statement

No competing financial interests exist.

References

1. Arnold WP, Mittal CK, Katsuki S, and Murad F. Nitric oxide activates guanylate cyclase and increases guanosine 3′:5′-cyclic monophosphate levels in various tissue preparations. *Proc Natl Acad Sci USA* 74: 3203–3207, 1977.
2. Battiato I, Tartakovsky DM, Tartakovsky AM, and Scheibe T. On breakdown of macroscopic models of mixing-controlled heterogeneous reactions in porous media. *Adv Water Resour* 32: 1664–1673, 2009.
3. Buerk DG. Can we model nitric oxide biotransport? A survey of mathematical models for a simple diatomic molecule with surprisingly complex biological activity. *Ann Rev Biomed Eng* 3: 109–143, 2001.
4. Butler AR, Megson IL, and Wright PG. Diffusion of nitric oxide and scavenging by blood in the vasculature. *Biochem Biophys Acta* 1425: 168–176, 1998.
5. Chen X, Jaron D, Barbee KA, and Buerk DG. The influence of radial RBC distribution, blood velocity profiles, and glycocalyx on coupled NO/O2 transport. *J Appl Physiol* 100: 482–492, 2006.
6. Cheng C, Tempel D, Oostlander A, Helderman F, Gijsen F, Wentzel J, van Haperen R, Haitsma DB, Serruys PW, van der Steen AF, de Crom R, and Krams R. Rapamycin modulates the eNOS vs. shear stress relationship. *Cardiovasc Res* 78: 123–129, 2008.
7. Cokelet GR and Goldsmith HL. Decreased hydrodynamic resistance in the two-phase flow of blood through small vertical tubes at low flow rates. *Circ Res* 68: 1–17, 1991.
8. Fischkoff S and Vanderkooi JM. Oxygen diffusion in biological and artificial membranes determined by the fluorochrome pyrene. *J Gen Physiol* 65: 663–676, 1975.
9. Gundersen SI, Chen G, and Palmer AF. Mathematical model of NO and O2 transport in an arteriole facilitated by hemoglobin based O2 carriers. *Biophys Chem* 143: 1–17, 2009.
10. Intaglietta M, Johnson PC, and Winslow RM. Microvascular and tissue oxygen distribution. *Cardiovasc Res* 32: 632–643, 1996.
11. Kavdia M and Popel AS. Wall shear stress differentially affects NO level in arterioles for volume expanders and Hb-based O2 carriers. *Microvasc Res* 66: 49–58, 2003.
12. Kim S, Kong RL, Popel AS, Intaglietta M, and Johnson PC. A computer-based method for determination of the cell-free layer width in microcirculation. *Microcirculation* 13: 199–207, 2006.
13. Lamkin-Kennard KA, Buerk DG, and Jaron D. Interactions between NO and O2 in the microcirculation: a mathematical analysis. *Microvasc Res* 68: 38–50, 2004.
14. Lancaster JR. Simulation of the diffusion and reaction of endogenously produced nitric oxide. *Proc Natl Acad Sci USA* 91: 8137–8141, 1994.
15. Mahler M, Louy C, Homsher E, and Peskoff A. Reappraisal of diffusion, solubility, and consumption of oxygen in frog skeletal muscle, with applications to muscle energy balance. *J Gen Physiol* 86: 105–134, 1985.
16. Malinski T, Taha Z, Grunfeld S, Patton S, Kapturczak M, and Tomboulian P. Diffusion of nitric oxide in the aorta wall monitored *in situ* by porphyrinic microsensors. *Biochem Biophys Res Commun* 193: 1076–1082, 1993.
17. Martini J, Carpentier B, Chavez Negrete A, Frangos JA, and Intaglietta M. Paradoxical hypotension following increased hematocrit and blood viscosity. *Am J Physiol Heart Circ Physiol* 289: H2136–H2143, 2005.
18. Martini J, Tsai AG, Cabrales P, Johnson PC, and Intaglietta M. Increased cardiac output and microvascular blood flow during mild hemoconcentration in hamster window model. *Am J Physiol Heart Circ Physiol* 291: H310–H317, 2006.
19. Mashour GA and Boock RJ. Effects of shear stress on nitric oxide levels of human cerebral endothelial cells cultured in an artificial capillary system. *Brain Res* 842: 233–238, 1999.
20. McAllister TN and Frangos JA. Steady and transient fluid shear stress stimulate NO release in osteoblasts through distinct biochemical pathways. *J Bone Mineral Res* 14: 930–936, 1999.
21. Nathan C. Nitric oxide as a secretory product of mammalian cells. *FASEB J* 6: 3051–3064, 1992.
22. Pozrikidis C. *Numerical Computation in Science and Engineering*, 2nd edition. New York: Oxford University Press, 2008.
23. Pries AR, Neuhaus D, and Gaehtgens P. Blood viscosity in tube flow: dependence on diameter and hematocrit. *Am J Physiol* 263: H1770–H1778, 1992.
24. Roy B and Garthwaite J. Nitric oxide activation of guanylyl cyclase in cells revisited. *Proc Natl Acad Sci USA* 103: 12185–12190, 2006.
25. Salazar Vázquez BY, Cabrales P, Tsai AG, Johnson PC, and Intaglietta M. Lowering of blood pressure by increasing hematocrit with non nitric oxide scavenging red blood cells. *Am J Respir Cell Mol Biol* 38: 135–142, 2008.
26. Sharan M and Popel AS. A two-phase model for flow of blood in narrow tubes with increased effective viscosity near the wall. *Biorheology* 38: 415–428, 2001.
27. Tartakovsky AM, Tartakovsky DM, Scheibe TD, and Meakin P. Hybrid simulations of reaction-diffusion systems in porous media. *SIAM J Sci Comput* 30: 2799–2816, 2008.
28. Tsoukias NM. Nitric oxide bioavailability in the microcirculation: insights from mathematical models. *Microcirculation* 15: 813–834, 2008.
29. Tsoukias NM and Popel AS. Erythrocyte consumption of nitric oxide in presence and absence of plasma-based hemoglobin. *Am J Physiol Heart Circ Physiol* 282: H2265–H2277, 2002.
30. Wang WC. A jump condition capturing finite difference scheme for elliptic interface problems. *SIAM J Sci Comput* 25: 1479–1496, 2004.
31. Weinbaum S, Tarbell JM, and Damiano ER. The structure and function of the endothelial glycocalyx layer. *Annu Rev Biomed Eng* 9: 121–167, 2007.
32. Weinbaum S, Zhang X, Han Y, Vink H, and Cowin SC. Mechanotransduction and flow across the endothelial glycocalyx. *Proc Natl Acad Sci USA* 100: 7988–7995, 2003.
33. Yalcin O, Choi C, Chatpun S, Intaglietta M, and Johnson PC. The dependence of cell-free layer thickness in arterioles on systemic hematocrit level. *FASEB J* 23: 949.7 (Abstract), 2009.

Address correspondence to:
Prof. Marcos Intaglietta
Department of Bioengineering
University of California, San Diego
9500 Gilman Dr.
La Jolla, CA 92093-0412

E-mail: mintagli@ucsd.edu

Date of first submission to ARS Central, April 23, 2010; date of final revised submission, May 25, 2010; date of acceptance, June 19, 2010.

Abbreviations Used

CFL = cell-free layer
D = diffusion coefficient
Hb = hemoglobin
Hct = hematocrit
NO = nitric oxide
O2 = oxygen
RBC = red blood cell

This article has been cited by:

1. X. Liu, Y. Fan, X. Y. Xu, X. Deng. 2012. Nitric oxide transport in an axisymmetric stenosis. *Journal of The Royal Society Interface* **9**:75, 2468-2478. [CrossRef]
2. Sang Woo Park, Marcos Intaglietta, Daniel M. Tartakovsky. 2012. Impact of endothelium roughness on blood flow. *Journal of Theoretical Biology* **300**, 152-160. [CrossRef]
3. Yipin Zhou, Pedro Cabrales, Andre F. Palmer. 2012. Simulation of NO and O2 transport facilitated by polymerized hemoglobin solutions in an arteriole that takes into account wall shear stress-induced NO production. *Biophysical Chemistry* . [CrossRef]
4. Peng Kai Ong, Seungkwan Cho, Bumseok Namgung, Sangho Kim. 2011. Effects of cell-free layer formation on NO/O2 bioavailability in small arterioles. *Microvascular Research* . [CrossRef]
5. C. Makena Hightower, Beatriz Y. Salazar Vázquez, Sung Woo Park, Krishna Sriram, Judith Martini, Ozlem Yalcin, Amy G. Tsai, Pedro Cabrales, Daniel M. Tartakovsky, Paul C. Johnson, Marcos Intaglietta. 2011. Integration of cardiovascular regulation by the blood/endothelium cell-free layer. *Wiley Interdisciplinary Reviews: Systems Biology and Medicine* **3**:4, 458-470. [CrossRef]
6. Peng Kai Ong, Swati Jain, Sangho Kim. 2011. Temporal variations of the cell-free layer width may enhance NO bioavailability in small arterioles: Effects of erythrocyte aggregation. *Microvascular Research* **81**:3, 303-312. [CrossRef]